

## Phase irregularity: A conceptually simple and efficient approach to characterize electroencephalographic recordings from epilepsy patients

Anaïs Espinosa <sup>\*</sup>

*Department of Information and Communication Technologies, Universitat Pompeu Fabra,  
Carrer Roc Boronat 138, 08018 Barcelona, Catalonia, Spain  
and Institute for Bioengineering of Catalonia (IBEC), The Barcelona Institute of Science and Technology,  
Carrer Baldiri Reixac 10-12, 08028 Barcelona, Catalonia, Spain*

Ralph G. Andrzejak 

*Department of Information and Communication Technologies, Universitat Pompeu Fabra, Carrer Roc Boronat 138,  
08018 Barcelona, Catalonia, Spain*



(Received 17 November 2021; accepted 6 March 2022; published 29 March 2022)

The severe neurological disorder epilepsy affects almost 1% of the world population. For patients who suffer from pharmacoresistant focal-onset epilepsy, electroencephalographic (EEG) recordings are essential for the localization of the brain area where seizures start. Apart from the visual inspection of the recordings, quantitative EEG signal analysis techniques proved to be useful for this purpose. Among other features, regularity versus irregularity and phase coherence versus phase independence allowed characterizing brain dynamics from the measured EEG signals. Can phase irregularities also characterize brain dynamics? To address this question, we use the univariate coefficient of phase velocity variation, defined as the ratio of phase velocity standard deviation and the mean phase velocity. Beyond that, as a bivariate measure we use the classical mean phase coherence to quantify the degree of phase locking. All phase-based measures are combined with surrogates to test null hypotheses about the dynamics underlying the signals. In the first part of our analysis, we use the Rössler model system to study our approach under controlled conditions. In the second part, we use the Bern-Barcelona EEG database which consists of focal and nonfocal signals extracted from seizure-free recordings. Focal signals are recorded from brain areas where the first seizure EEG signal changes can be detected, and nonfocal signals are recorded from areas that are not involved in the seizure at its onset. Our results show that focal signals have less phase variability and more phase coherence than nonfocal signals. Once combined with surrogates, the mean phase velocity proved to have the highest discriminative power between focal and nonfocal signals. In conclusion, conceptually simple and easy to compute phase-based measures can help to detect features induced by epilepsy from EEG signals. This holds not only for the classical mean phase coherence but even more so for univariate measures of phase irregularity.

DOI: [10.1103/PhysRevE.105.034212](https://doi.org/10.1103/PhysRevE.105.034212)

### I. INTRODUCTION

Epilepsy is one of the most common neurological disorders. It is characterized by epileptic seizures which are related to abnormal excessive neuronal activity in the brain [1]. For patients who suffer from pharmacoresistant focal-onset epilepsy (around 9% of all epilepsy patients [2]), a potential therapy is the neurosurgical resection of the brain area where seizures start [2,3]. To plan epilepsy surgery, the precise localization of this brain area is crucial. For this purpose intracranial multichannel electroencephalographic (EEG) recordings play an important role [4,5]. In particular, one has to identify those channels where the first seizure EEG signal changes can be detected. In this study, we analyze signals recorded during the seizure-free interval from these focal channels as well as from nonfocal signals which are recorded

from brain areas that are not involved in the seizure at its onset. Nowadays, the visual inspection of these EEG recordings by clinicians is complemented by quantitative EEG signal analysis techniques [6–46]. The aim of this multidisciplinary analysis is to understand how epilepsy affects the dynamics of the brain and help to arrive at valuable diagnostic information. From a physics perspective, the dynamics of the brain area where the seizure starts is altered, not only during seizures [6–21] but also during seizure-free intervals [6–9,13,22–46]. Thus, the analysis of seizure-free EEG recordings can complement other techniques [47,48] in the diagnostics of epilepsy patients. In order to promote the study of epilepsy, researchers provide public domain EEG databases. In this study, we use the Bern-Barcelona database, available in Ref. [49].

The Bern-Barcelona database was constructed and first analyzed by Andrzejak *et al.* [39] applying univariate and bivariate nonlinear signal analysis techniques. The measures were used together with the concept of surrogates to test specific null hypotheses about the underlying dynam-

<sup>\*</sup>anais.espinosa@gmail.com

ics [50]. The database contains focal and nonfocal signals from seizure-free EEG recordings of patients suffering from pharmacoresistant focal-onset epilepsy. These two groups of signals demonstrated to have different dynamical characteristics. For instance, determinism, nonlinear interdependence, and stationarity were more evident in focal signals. Subramaniam *et al.* [51] used recurrence network measures together with surrogates which, in contrast to those used in Ref. [39], preserve the dynamics' nonstationarity. Their results showed high levels of structural complexity and interdependence in focal signals. Sharma *et al.* classified focal and nonfocal signals by applying machine learning to different entropy features [52–54]. In a recent study [54], Sharma *et al.* achieved a diagnostic accuracy of 95%. Acharya *et al.* [55] reviewed articles that used the Bern-Barcelona database and proposed a computer-aided system for the detection of focal and nonfocal signals.

An approach to distinguish focal and nonfocal signals is the characterization of the dynamics' regularity versus irregularity [9,39,43,55–60] and interdependence versus independence [23,38,39,51,61,62]. The study of irregularity [63–69] and independence [70–73] can furthermore yield beneficial information in the study of other neurological diseases. The features of irregularity and independence are often computed by time-consuming signal analysis techniques, and computation time is particularly relevant when applied to long signals or big databases. Moreover, these techniques are sometimes difficult to interpret and several intermediate steps are needed to reach the final result. Moreover, one has to be careful with the selection of the primary observable used as input for the signal analysis. EEG recordings are usually influenced by the impedance between the electrodes and tissue and can be affected by different artifacts of physiological or technical origin during the measurement. Accordingly, EEG amplitude signals are sometimes not very reliable, and signals of instantaneous EEG phases can be more informative [74]. Beyond their application to EEG signals [38,75–78], instantaneous phase signals are used in different fields of signal processing: telecommunication systems [79,80], electrocardiography [81,82], and geophysics [83,84], among others. The instantaneous phase can be determined by means of several techniques, e.g., the Hilbert transform [85], complex wavelet transform [86], or the marker event method [87,88]. Here one should note that Quiñero *et al.* [89] showed that the Hilbert transform together with filtering leads to equivalent results like the wavelet method. After comparing these different techniques in some preanalysis, we decided to extract the phase using the Hilbert transform.

Since phase-based measures are conceptually simple and easy to compute, we use them in this study to analyze EEG signals from epilepsy patients to detect phase irregularities and phase synchronization. Phase irregularities are present in various nonlinear physiological systems, and their characterization is important to properly understand the functionality of the organism [90]. Phase synchronization can be useful for the study of physiological processes [91–93] as well as neuronal diseases [76,94,95]. In particular, phase synchronization was demonstrated to contribute to quantitative EEG analysis with respect to the dynamics of seizures [38,96–99], the seizure-free interval [31,32,38,96,100], and the distinction of focal

and nonfocal signals [38]. Therefore, the main question addressed in this study is the following. Given that the analysis of phase synchronization was demonstrated to contribute positively to the study of EEG signals, can phase irregularities also characterize brain dynamics? In particular, do they allow us to differentiate focal and nonfocal signals even in the absence of seizures?

To address this open question, we apply univariate and bivariate phase-based measures to the Bern-Barcelona database. The univariate measure *coefficient of phase velocity variation* is selected here to quantify phase irregularities of individual dynamics  $X$  from single signals  $x$ . This signal analysis technique is based on diffusion measures [90,101,102], which capture invariant phase characteristics. However, these measures cannot always be applied to empirical data since they use ensemble averages across independent realizations of the dynamics. In this study, we perform averages across time since we have only single signals, i.e., single realizations. As a bivariate approach, we use the *mean phase coherence* to quantify the degree of phase synchronization between two dynamics  $X$  and  $Y$  based on simultaneously measured signals  $x$  and  $y$  [38,103]. Following previous work [31,38,41,104–107], prior to applying these techniques to EEG recordings, we test them on the low-dimensional nonlinear Rössler model system. Despite that the Rössler dynamics is chaotic, it is narrow banded in the frequency domain and therefore its Hilbert phase is well defined. Accordingly, the Rössler model system is very well suited to test phase-based measures under controlled conditions. It should not, however, be mistaken for a model of brain dynamics. While brain dynamics are certainly not linear, they are not low dimensional, and EEG signals are typically not narrow banded. On the other hand, we reduce this gap somewhat in part of our analysis by adding dynamical noise to the Rössler dynamics to have a system more similar to real-world dynamics. We furthermore combine the phase-based measures with the concept of surrogates [8,45,50,108] to disentangle the impact of nonstationarities, nonlinearities, and correlations on our measures. Doing so, we design phase-based surrogate tests to study the consistency of the dynamics underlying focal and nonfocal signals with the surrogates' null hypothesis.

## II. MATERIALS AND METHODS

### A. Rössler dynamics

We analyze a pair of bidirectionally coupled Rössler dynamics [109] which is a widely used chaotic nonlinear model system [31,38,41,104–107]. The reason to select this model system is because its trajectory rotates around a single center. It is therefore straightforward to obtain the phase of the dynamics which allows us to evaluate the phase-based measures. For the purpose of the joined evaluation of the coefficient of phase velocity variation and the mean phase coherence we use a pair of two coupled Rössler dynamics with dynamical noise:

$$\begin{aligned}
 dx_1(t) &= (-\omega_x x_2(t) - x_3(t) \\
 &\quad + \epsilon_{y \rightarrow x}(y_1(t) - x_1(t)))dt + d\eta_x(t), \\
 dx_2(t) &= (\omega_x x_1(t) + 0.165x_2(t))dt + d\eta_x(t), \\
 dx_3(t) &= (0.2 + x_3(t)(x_1(t) - 10))dt,
 \end{aligned} \tag{1}$$

$$\begin{aligned}
dy_1(t) &= (-\omega_y y_2(t) - y_3(t) \\
&\quad + \epsilon_{x \rightarrow y}(x_1(t) - y_1(t)))dt + d\eta_y(t), \\
dy_2(t) &= (\omega_x y_1(t) + 0.165 y_2(t))dt + d\eta_x(t), \\
dy_3(t) &= (0.2 + y_3(t)(y_1(t) - 10))dt. \tag{2}
\end{aligned}$$

The dynamics are made nonidentical by using a mismatch in the natural frequencies  $\omega_x = 0.89$  and  $\omega_y = 0.85$ . Both systems are coupled with coupling strength  $\epsilon_{x \rightarrow y}$  from  $X \rightarrow Y$  and  $\epsilon_{y \rightarrow x}$  from  $Y \rightarrow X$ . The noise terms  $\eta_x$ ,  $\eta_y$  are independent Gaussian  $\delta$ -correlated noise with variance  $2O_{x,y}$  and zero mean:  $\langle \eta_{x,y}(t)\eta_{x,y}(t') \rangle = 2O_{x,y}\delta(t-t')\delta_{x,y}$ . Thus, the noise is uncorrelated for different times  $t \neq t'$ , and  $\eta_x$  and  $\eta_y$  are always uncorrelated between  $X$  and  $Y$  and between the first and second components. We apply noise only in the first and second component for each system but not in the third component which gives rise to the nonlinearity to the dynamics. This is done since in preanalysis we found that adding noise also to the third component quickly destabilized the system and therefore did not allow us to study sufficient noise level ranges. We define the noise level by the standard deviation of  $\eta_{x,y}$  which is given by  $\xi_{x,y} = \sqrt{2O_{x,y}}$ .

To integrate the dynamics we use the Euler method with step size  $dt = 0.001$  time units, where the noise is added in every integration step. In order to have approximately 20 points per cycle of the Rössler dynamics, we down-sample by a factor of 300, resulting in a sampling interval of  $\Delta t = 0.3$  time units. Starting from random initial conditions we integrate a total of 100 000 data points from which we use only the last 4096 data points to let transients fade away.

### B. Intracranial EEG recordings

As recordings from epilepsy patients we use the publicly available Bern-Barcelona EEG database [39], which consists of EEG recordings performed at the Department of Neurology of the University of Bern, Switzerland. These recordings were done using electrodes each equipped with several recording channels. These electrodes were implanted onto the surface of the brain or in deeper brain structures. These intracranial EEG recordings were obtained as part of the epilepsy diagnostics prior to epilepsy surgery. The database contains recordings from five patients suffering from pharmacoresistant focal-onset epilepsy. In all cases clinicians located the seizure onset in one of the two hemispheres. The recordings do not include any seizure episode. Instead, they are from seizure-free periods, i.e., the time between seizures. The data were filtered with a Butterworth filter between 0.5 and 150 Hz, and sampled at 512 Hz. EEG signals were then re-referenced against the median of all the channels free of permanent artifacts as judged by visual inspection.

The Bern-Barcelona database was constructed to contain only signals with a minimal amount of artifacts. It contains two types of signals. The first type are focal signals, which were recorded from brain areas where the first ictal EEG changes were detected. The second type are nonfocal signals, recorded from brain areas that were not involved in the seizure at its onset. In total the database contains 3750 pairs of focal signals and 3750 pairs of nonfocal signals. Each pair of signals, which we refer to as  $x$  and  $y$ , was simultaneously

recorded from neighboring channels on one electrode. For the univariate analysis we use only the signals  $x$ , whereas for the bivariate analysis we use the pair of signals  $x$  and  $y$ . Beyond this pairing and the information if the signals are focal or nonfocal, the database was designed such that the signals are randomized. In particular, the index of the signal pair is not related to the identity of the patient or recording location inside the patient's brain. Every signal has 20 s corresponding to 10 240 time points. We applied an eighth-order Butterworth low-pass filter with a cutoff frequency of 40 Hz and a 40th-order Butterworth stop-band filter between 46.5 and 53.5 Hz. This was done to work with the same preprocessing as performed in Ref. [39] for the nonlinear measures. For the last part of the analysis we applied a sixth-order Butterworth bandpass filter using the classical EEG frequency bands:  $\delta$  (0.5–4 Hz),  $\theta$  (4–8 Hz),  $\alpha$  (8–12 Hz), and  $\beta$  (12–31 Hz). Figure 1 shows some exemplary pairs of focal and nonfocal EEG signals.

### C. Phase of a signal

We use the *analytic signal concept* based on the Hilbert transform [85] to compute the instantaneous phase  $\phi(t)$ . Given a signal  $x(t)$  extracted from a system  $X$  we obtain the Hilbert transform  $x_{\mathcal{H}}(t)$  as

$$x_{\mathcal{H}}(t) = \text{p.v.} \int_{-\infty}^{+\infty} \frac{x(\tau)}{\pi(t-\tau)} d\tau, \tag{3}$$

where p.v. denotes that the integral is done following the Cauchy principal value. From Eq. (3) we see that  $x_{\mathcal{H}}(t)$  is a convolution of  $x(t)$  with  $\frac{1}{\pi t}$  in the time domain. In the frequency domain this convolution translates to the product of the complex-valued Fourier transforms. The Fourier transform of  $\frac{1}{\pi t}$  is

$$\mathcal{F}\left(\frac{1}{\pi t}\right) = \begin{cases} e^{i\frac{\omega}{2}} & \text{for } -\pi < \omega < 0 \\ 0 & \text{for } \omega = 0 \\ e^{-i\frac{\omega}{2}} & \text{for } 0 < \omega < \pi \end{cases}.$$

Recalling that the multiplication of two complex numbers corresponds to multiplying their absolute value and summing their phases and taking into account the Hermitian symmetry of the Fourier transform of real-valued signals, we can see that the Hilbert transform performs a shift of the original signal by  $\frac{1}{2}\pi$ , maintaining the power spectrum [110].

An analytic signal  $x_{\alpha}(t)$  can be expressed in the complex plane with an imaginary unit  $i$  as

$$x_{\alpha}(t) = x(t) + ix_{\mathcal{H}}(t) = A(t)e^{i\phi(t)}, \tag{4}$$

where  $\phi(t)$  is the instantaneous phase and  $A(t)$  is the instantaneous amplitude. Accordingly, we can extract  $\phi(t)$  by

$$\phi(t) = \arctan \frac{x_{\mathcal{H}}(t)}{x(t)}. \tag{5}$$

This function has values in the interval  $(-\pi, \pi]$ , and therefore provides the phase wrapped to this interval. We denote the continuous unwrapped phase by  $\Phi(t)$ .

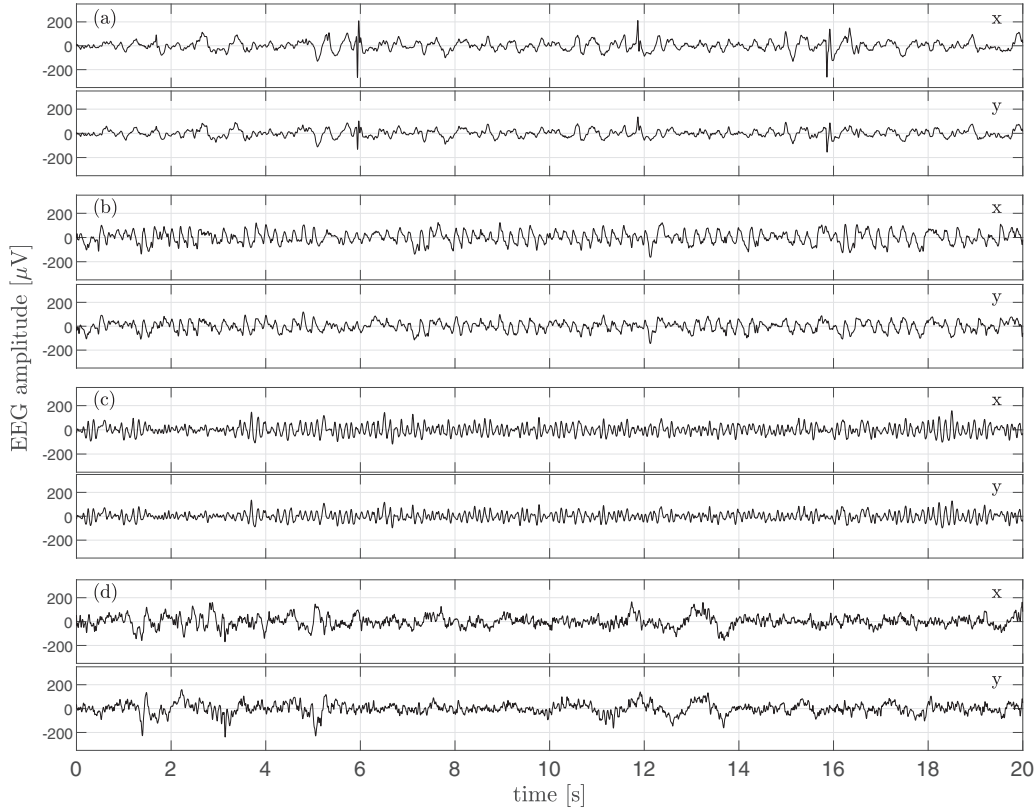


FIG. 1. Exemplary pairs of (a), (b) focal and (c), (d) nonfocal EEG signals.

#### D. Phase-based measures

To numerically determine the phase-based measures it is important to recall that we deal with signals consisting of  $N$  samples taken at discrete times  $t_j$  for  $j = 0, \dots, N-1$  separated by the sampling interval  $\Delta t = t_{j+1} - t_j$ .

##### 1. Coefficient of phase velocity variation

We use the univariate coefficient of phase velocity variation to characterize the irregularity of the individual dynamics  $X$  based on measured signals  $x$ . For this purpose we analyze the unwrapped phase  $\Phi(t)$ . As the first step we define the instantaneous phase velocity  $\Omega(t_j)$  [111–113],

$$\Omega(t_j) = \frac{\Phi(t_{j+1}) - \Phi(t_j)}{\Delta t}, \quad (6)$$

the mean phase velocity  $M$ ,

$$M = \mu \langle \Omega(t_j) \rangle_{j=0, \dots, N-1}, \quad (7)$$

and the phase velocity standard deviation  $S$ ,

$$S = \sigma \langle \Omega(t_j) \rangle_{j=0, \dots, N-1}, \quad (8)$$

across the range of time indices indicated at the angular brackets. To quantify deviations from the linear growth of the phase we use the coefficient of phase velocity variation  $V$ :

$$V = \frac{S}{M}. \quad (9)$$

In our study, all systems are defined such that the mean phase velocity  $M$  is positive. Furthermore, the phase velocity standard deviation  $S$  cannot be negative. Accordingly, the lowest

bound of  $V$  is zero, which is attained if and only if  $\Omega(t_j)$  is constant across  $j = 0, \dots, N-1$ . However, despite that the coefficient of phase velocity variation  $V$  is divided by the mean phase velocity  $M$ , it is neither normalized to one nor bounded from above. We refer to the measures as such using the corresponding symbols:  $V$ ,  $M$ , and  $S$ . Whenever referring to a specific system or signal, we add a subindex to the symbol. For instance,  $V_x$  is used for coefficient of phase velocity variation values of system  $X$ .

As examples, we use unwrapped phases  $\Phi(t)$  extracted from exemplary signals from Rössler dynamics [Fig. 2(a)] and EEG recordings [Fig. 2(b)], which result in intermediate values of  $V$ . For the Rössler dynamics we get nonzero values of  $S$  even in the absence of noise. The source of this phase irregularity is the nonlinearity of the Rössler dynamics. Once we add noise to the dynamics, the deviations from the linear growth of  $\Phi(t)$  are higher, leading to increased values of  $S$ . In contrast, in this example the mean phase velocity  $M$  is not strongly affected by noise, and the increase of  $S$  directly results in an increase of  $V$ . In summary, the case of the Rössler dynamics shows that noise and/or nonlinearity can be source of the phase irregularity as assessed by  $V$ .

Contrary to the Rössler examples [Fig. 2(a)], we see a low and a high average slope in the unwrapped phases  $\Phi(t)$  of two EEG signals [Fig. 2(b)], resulting in differing values of  $M$  for these two examples. For the EEG signals we also have different values of  $V$ , similar to what we observe for the Rössler dynamics. While the source of increased values  $S$  in the Rössler dynamics can be noise and/or nonlinearity, for the EEG signals it captures these and any other source of phase

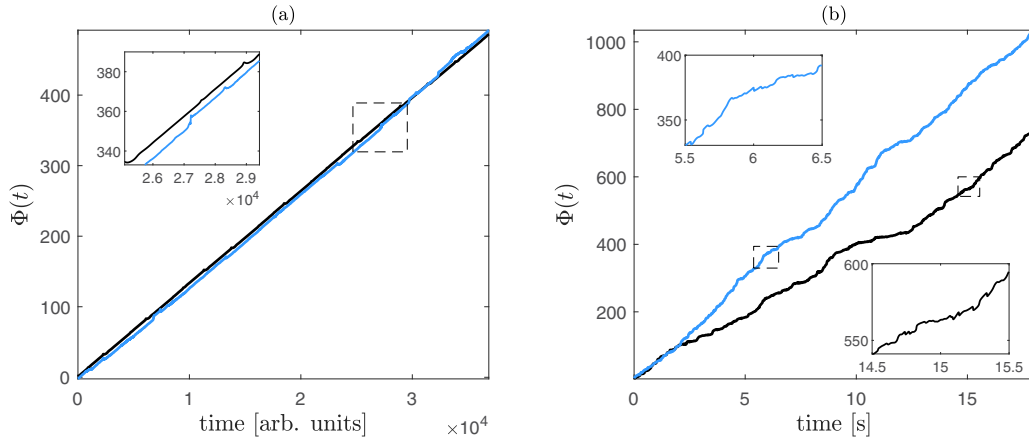


FIG. 2. Any deviation of  $\Phi(t)$  from the linear growth is detected by the coefficient of phase velocity variation  $V$ . (a) Unwrapped phases  $\Phi(t)$  in a noise-free Rössler dynamics (black) and in a noisy Rössler dynamics (blue) with noise level  $\xi = 1$ . The inset shows a zoom into the dashed rectangle. The coefficients of phase velocity variation  $V$  for these examples are  $V_{\text{black}} = 0.29$  and  $V_{\text{blue}} = 1.43$ . Values of mean phase velocity:  $M_{\text{black}} = 0.044$  and  $M_{\text{blue}} = 0.045$ . Values of phase velocity standard deviation:  $S_{\text{black}} = 0.013$  and  $S_{\text{blue}} = 0.064$ . (b) Same as panel (a) but for unwrapped phases  $\Phi(t)$  of two EEG signals (black and blue). Results for these examples are as follows. Coefficient of phase velocity variation:  $V_{\text{black}} = 2.18$  and  $V_{\text{blue}} = 1.66$ . Mean phase velocity:  $M_{\text{black}} = 0.080$  and  $M_{\text{blue}} = 0.112$ . Standard deviation velocity:  $S_{\text{black}} = 0.175$  and  $S_{\text{blue}} = 0.186$ .

deviations. Recall from Eq. (9) that to compute the coefficient of phase velocity variation  $V$ , values of  $S$  are divided by the mean phase velocity  $M$ . Therefore, these particular examples show that an increase of  $S$  does not necessarily have to result in higher values of  $V$ .

The phase velocity standard deviation  $S$  and thereby the coefficient of phase velocity variation  $V$  are based on diffusion measures [90,101,102]. However, these diffusion measures are typically based on ensemble averages across different realizations of the dynamics. In our setting we only have individual realizations for each of our signals, and we therefore perform averages across time. We are aware that the assumptions of stationarity and ergodicity which in principle underlie temporal instead of ensemble averages are not fulfilled. This does not invalidate our approach since we aim to characterize any possible deviation from the strictly linear phase growth, which can also include the degree to which the assumption of stationarity is not fulfilled. Our averages across time also avoid the necessity to use sophisticated techniques like in Ref. [90].

**2. Mean phase coherence**

The mean phase coherence  $R$  quantifies the degree of phase locking between two dynamics  $X$  and  $Y$ . We use the steps described in Sec. II C to extract the instantaneous phases,  $\phi_x(t)$  and  $\phi_y(t)$ , from the signals  $x(t)$  and  $y(t)$ , respectively, and determine the relative phase difference  $\varphi(t)$ :

$$\varphi(t) = \phi_x(t) - \phi_y(t). \tag{10}$$

To measure the mean phase coherence, we assess the distribution of phase differences  $\varphi(t)$  by means of the order parameter [38,94,103]:

$$R = \left| \frac{1}{N} \sum_{j=0}^{N-1} e^{i\varphi(t_j)} \right|. \tag{11}$$

The measure  $R$  is bounded in the interval  $[0,1]$ . If both dynamics are independent,  $R$  takes values close to zero. Only when  $N$  goes to  $\infty$ ,  $R$  goes to zero. In contrast, when we have strong phase locking, meaning that the relative phase difference  $\varphi(t)$  is constant during all time  $t$ , we obtain  $R = 1$ . In between these two boundaries, low and high values of  $R$  indicate a weak and strong degree of phase synchronization, respectively. For dynamics such as the Rössler [Eqs. (1) and (2)], higher values of coupling typically lead to higher values of phase synchronization and thereby higher values of  $R$ . The stronger the mismatch in the natural frequencies, the stronger needs to be the coupling to obtain phase synchronization [87,114].

**E. Surrogates**

As stated above, for independent dynamics values of the mean phase coherence  $R$  go to zero only for  $N$  to infinity. However, in real-world data we never have an infinite number of data points. Therefore, we do not know which values of  $R$  to expect for independent dynamics. Furthermore, we cannot know how the auto- and cross-correlations of the signals influence  $R$ . Similarly, we do not know which values of  $V$  to expect if the only source of phase irregularity is the stochasticity of the dynamics or measurement noise in the signals. To address this problem, we can estimate values for  $R$  and  $V$  expected under certain null hypotheses using surrogate signals [50].

The concept of surrogates allows us to test a broad variety of null hypotheses  $H_0$  about the dynamics underlying measured signals [50]. Surrogate signals are random versions of original signals which maintain selected properties and destroy others by a constrained randomization process. Therefore, depending on the  $H_0$  we want to test, we use surrogates which maintain different properties.

In this study, we use univariate and bivariate *iterative amplitude adjusted Fourier transform* (IAAFT) surrogates [115]. Univariate surrogates have the same amplitude distribution

and autocorrelation that is practically indistinguishable from the one of the individual original signals  $x$ . The  $H_0^{\text{uni}}$  represented by these surrogates is that the dynamics  $X$  is a univariate stationary linear stochastic autocorrelated Gaussian process [39,115]. Furthermore, we use bivariate surrogates which have the same autocorrelation, cross-correlation, and amplitude distributions as the original pairs of signals  $x$  and  $y$ . The  $H_0^{\text{bi}}$  represented by bivariate surrogates is that the dynamics  $X$  and  $Y$  are a bivariate stationary linear stochastic auto- and cross-correlated Gaussian process [39,116–118]. In both cases, the measurement function by which the signals are derived from the dynamics is assumed to be invertible but potentially nonlinear, leading to non-Gaussian amplitude distributions.

### F. Testing procedure

To perform a univariate phase-based test, we calculate the coefficient of phase velocity variation  $V$  [Eq. (9)], the mean phase velocity  $M$  [Eq. (7)], and the phase velocity standard deviation  $S$  [Eq. (8)] for the original time series and 19 univariate surrogates. We denote these tests as  $\mathcal{V}$ ,  $\mathcal{M}$ , and  $\mathcal{S}$ , respectively. For each measure separately we reject  $H_0^{\text{uni}}$  by means of the corresponding test if the result from the original signal is lower than the minimal value from the set of surrogates (significance level  $\alpha = 0.05$ ). To denote the fraction of times we get a rejection we use the symbols  $\mathcal{V}$ ,  $\mathcal{M}$ , and  $\mathcal{S}$  with the subindex 1. Whenever needed we use an additional subindex to distinguish between systems or signal types. For instance,  $\mathcal{V}_{x,1}$  means the fraction of rejections in system  $X$ , and  $\mathcal{M}_{f,1}$  denotes the fraction of rejections for focal signals.

We run a bivariate phase-based test, determining the mean phase coherence  $R$  [Eq. (11)] for the pair of original signals  $x$  and  $y$  and 19 pairs of bivariate surrogate signals. We reject  $H_0^{\text{bi}}$  of this mean phase coherence test  $\mathcal{R}$  if  $R$  for the original signal pair is higher than the maximal  $R$  value from the set of bivariate surrogate signal pairs ( $\alpha = 0.05$ ). We use  $\mathcal{R}_1$  to denote the fraction of times we get a rejection. Unlike in the case of univariate phase-based tests, since we are working with pairs of signals, we do not have to include subindices to distinguish between systems  $X$  and  $Y$ , but only for focal and nonfocal signals.

Results for exemplary pairs of EEG signals are as follows: Fig. 1(a), rejection of univariate tests and bivariate test; Fig. 1(b), rejection of univariate tests and no rejection of bivariate test; Fig. 1(c), no rejection of univariate tests and bivariate test; and Fig. 1(d), no rejection of univariate tests and rejection of bivariate test. The same outcomes are obtained for signals  $x$  and  $y$ . In our study for univariate phase-based tests we just work with signal  $x$ .

## III. RESULTS

### A. Phase-based measures in Rössler dynamics

In this section we study under controlled conditions how noise affects the phase-based measures in model dynamics. Figure 3 shows the coefficient of phase velocity variation  $V$  and the mean phase coherence  $R$  applied to a pair of coupled nonidentical Rössler dynamics for different noise levels  $0 \leq \xi_{x,y} \leq 2$ . These results are averaged across 50 realizations.

For Figs. 3(a)–3(c) we apply bidirectional coupling  $\epsilon_{y \rightarrow x} = \epsilon_{x \rightarrow y} = 1$ , i.e., with the same strength in both directions [Eqs. (1) and (2)]. Even in the absence of noise ( $\xi_{x,y} = 0$ ), the coefficient of phase velocity variation  $V$  attains nonzero values. This result of  $V$  reflects irregularities in the phases which are caused by nonlinearities of the Rössler dynamics. Despite the irregularity of individual phases we get strong locking between them as detected by the mean phase coherence  $R$  equal to 1 for the noise-free case. Upon increasing  $\xi_{x,y}$ , we obtain higher values of  $V_{x,y}$  and lower values of  $R$ , reflecting the increased phase irregularity and decreased phase coherence, respectively. For system  $X$  [Fig. 3(a)], we obtain increased values of  $V_x$  for higher values of  $\xi_x$ . Moreover, due to the coupling  $\epsilon_{y \rightarrow x}$ , higher values of  $V_x$  are also obtained for higher values of  $\xi_y$ . An analogous situation is found with the role of systems  $X$  and  $Y$  exchanged [Fig. 3(b)]. Results from Figs. 3(a) and 3(b) are different due to the mismatch of both systems in their natural frequencies.

The results illustrating the influence of dynamical noise on Rössler dynamics using bidirectional coupling with unequal coupling strengths in the two directions are shown in Figs. 3(d)–3(f). The coupling strength  $\epsilon_{x \rightarrow y} = 2$  is higher as compared to the previous analysis shown in Figs. 3(a)–3(c). As a consequence of this stronger influence of the system  $X$  on the system  $Y$ , increasing the values of  $\xi_x$  leads to higher values of  $V_y$  [compare Fig. 3(e) to Fig. 3(b)]. In contrast, in system  $X$  [Fig. 3(d)] the increase of the noise in the opposite system  $\xi_y$  increases  $V_x$  to a lesser degree as compared to the results obtained for bidirectional coupling with equal strengths [Fig. 3(a)]. Finally, the results of  $R$  in this simulation are not affected strongly by the increase of  $\epsilon_{x \rightarrow y}$  [compare Fig. 3(f) to Fig. 3(c)].

Now we consider the case of unidirectional coupling, where system  $X$  has an effect on system  $Y$  via  $\epsilon_{x \rightarrow y} = 1.5$ , but receives no feedback from it because  $\epsilon_{y \rightarrow x} = 0$  [Figs. 3(g)–3(i)]. Therefore, values of  $V_x$  are not affected by changes in the noise level in the opposite system  $\xi_y$  [Fig. 3(g)]. With regard to system  $Y$ , higher values of  $\xi_x$  cause higher values of  $V_y$  but only for values of  $\xi_y$  below approximately 1 [Fig. 3(h)]. On the contrary, for values of  $\xi_y$  higher than 1, the increase of  $V_y$  is not monotonic with regard to increasing noise  $\xi_x$ . For example, at  $\xi_y = 1.5$  and increasing values of  $\xi_x$  up to 0.7,  $V_y$  at first decreases. Then, for values of  $\xi_x$  higher than 0.7,  $V_y$  increases. The results of  $R$  [Fig. 3(i)] are qualitatively very similar to the ones from  $V_y$  [Fig. 3(h)].

Accordingly, in this third setting of the coupling we find that for a certain range of noise levels, more noise leads to less phase irregularity and more phase synchronization. This behavior resembles the stochastic resonance phenomenon, which occurs in nonlinear systems when noise can enhance the phase coherence between two dynamics [119]. Recall that our two Rössler systems are nonidentical in their natural frequencies, and in this setting the system with the higher natural frequency (system  $X$ ) is the one driving the system exhibiting stochastic resonance (system  $Y$ ). If we drive the faster system  $X$  with the slower system  $Y$ , we do not get stochastic resonance (results not shown). This is in accordance with Ref. [120], because a particular match between the driving frequency and the range of noise levels is needed to get stochastic resonance.

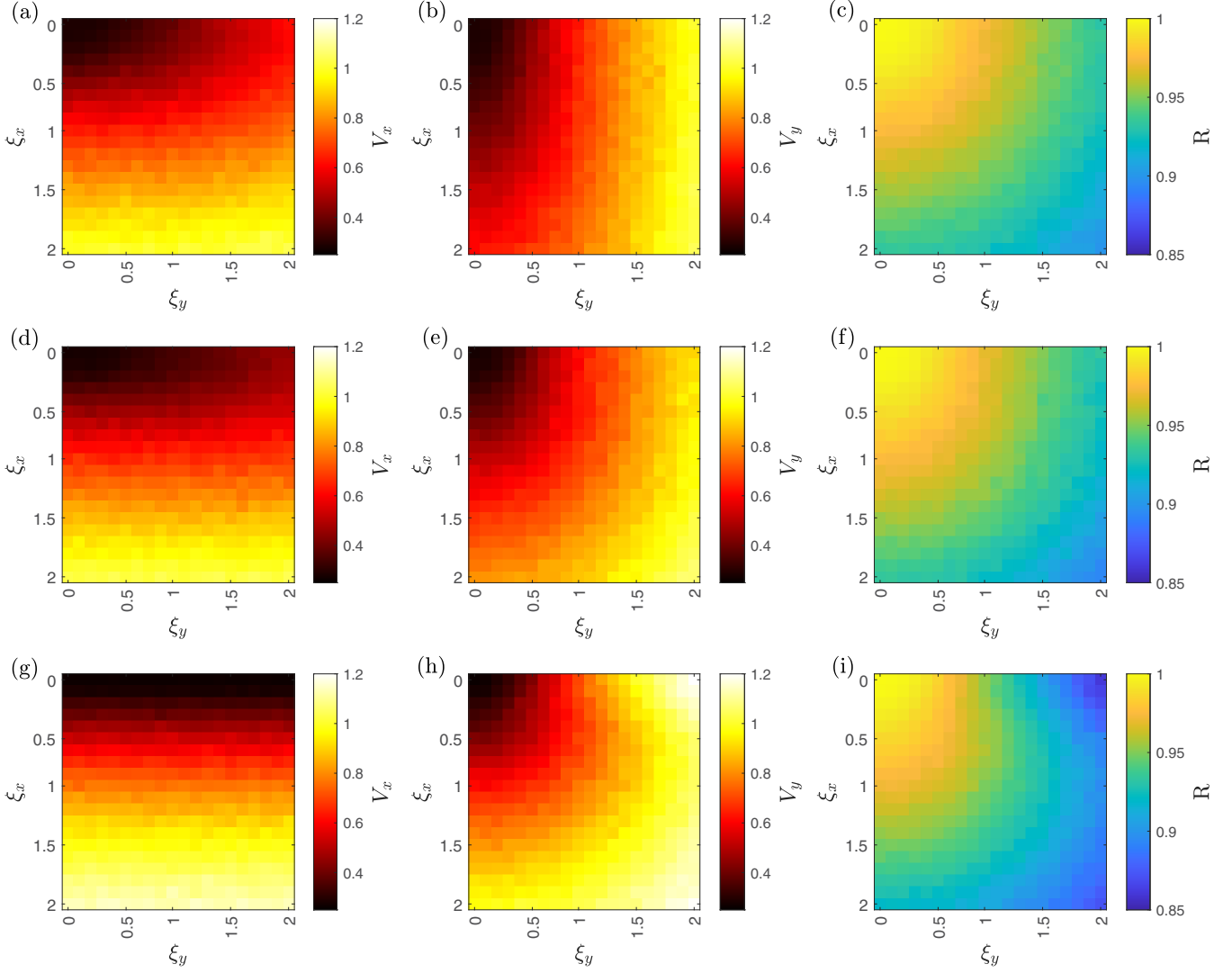


FIG. 3. While in general higher levels of noise  $\xi_{x,y}$  lead to higher values of the coefficient of phase velocity variation  $V$  and lower values of the mean phase coherence  $R$ , we also find results resembling stochastic resonance. Mean values of  $V$  and  $R$  are obtained from 50 realizations of two coupled noisy nonidentical Rössler dynamics in dependence on the noise levels  $\xi_{x,y}$ . (a)–(c) Bidirectional coupling with equal coupling strengths  $\epsilon_{x \rightarrow y} = \epsilon_{y \rightarrow x} = 1$ . (d)–(f) Bidirectional coupling with unequal coupling strengths  $\epsilon_{x \rightarrow y} = 2$  and  $\epsilon_{y \rightarrow x} = 1$ . (g)–(i) Unidirectional coupling  $\epsilon_{x \rightarrow y} = 1.5$  and  $\epsilon_{y \rightarrow x} = 0$ . Panels (a), (d), and (g) show values of the coefficient of phase velocity variation for system  $X$  ( $V_x$ ). The corresponding results for system  $Y$  ( $V_y$ ) are shown in (b), (e), and (h). Panels (c), (f), and (i) represent values of  $R$  quantifying the mean phase coherence between systems  $X$  and  $Y$ .

### B. Hypothesis testing for Rössler dynamics

We now extend the simulation based on bidirectional coupling with unequal coupling strengths [see again Figs. 3(d)–3(f)]. For each noise level  $\xi_{x,y}$  and each of the 50 realizations, we carry out the tests  $\mathcal{V}$ ,  $\mathcal{M}$ , and  $\mathcal{S}$  for signal  $x$ . Recall from Sec. II F that these tests consist of combining each of the univariate phase-based measures ( $V$ ,  $M$ , and  $S$ ) with univariate surrogates to test the null hypothesis  $H_0^{\text{uni}}$  of a stationary linear stochastic autocorrelated Gaussian process measured by an invertible but potentially nonlinear measurement function. This allows us to compare the sensitivity of the measures for the alternative hypothesis, since  $H_0^{\text{uni}}$  is not correct for the Rössler dynamics.

Results of the measures ( $V_x$ ,  $M_x$ , and  $S_x$ ) and the fractions of times we get a rejection for the tests ( $\mathcal{V}_{x,1}$ ,  $\mathcal{M}_{x,1}$ , and  $\mathcal{S}_{x,1}$ )

are shown in Fig. 4. As a consequence, Fig. 4(a) is a replica of Fig. 3(d). Comparing rejection rates, the overall highest values are obtained for  $\mathcal{M}_{x,1}$ , followed by  $\mathcal{S}_{x,1}$  and then  $\mathcal{V}_{x,1}$ . Accordingly,  $M$  has the highest sensitivity for the complement of  $H_0^{\text{uni}}$ . In all three cases, for higher values of noise we get less rejections of  $H_0^{\text{uni}}$ . When the null hypothesis was not rejected we found that the result for the original signal was typically within the results for the set of surrogate signals. Only for two combinations of noise levels was  $V_x$  for the original signal higher than for the maximum of the set of surrogates (results not shown).

To understand the test outcomes, we look at the values of  $V_x$ ,  $M_x$ , and  $S_x$  in Figs. 4(a)–4(c). As we pointed out in Sec. III A, higher noise levels  $\xi_x$  lead to higher values of the coefficient of phase velocity variation  $V_x$  [Fig. 4(a)]. Since

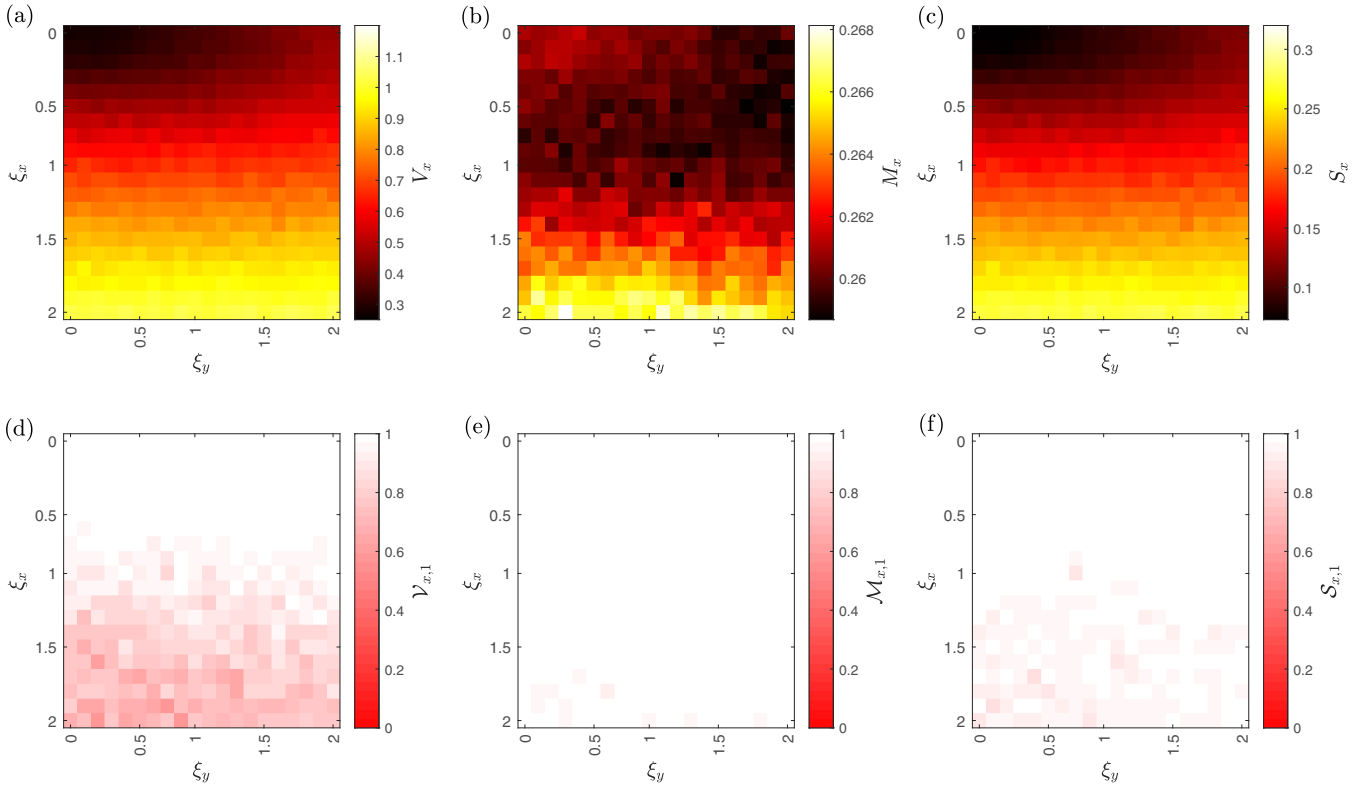


FIG. 4. The measure mean phase velocity  $M$  shows higher robustness against noise as compared to the coefficient of phase velocity variation  $V$  and phase velocity standard deviation  $S$ . (a)–(c) Mean values of  $V_x$ ,  $M_x$ , and  $S_x$  from 50 realizations of two coupled nonidentical Rössler dynamics in dependence on the noise levels  $\xi_{x,y}$ . We here use bidirectional coupling with unequal coupling strengths:  $\epsilon_{x \rightarrow y} = 2$  and  $\epsilon_{y \rightarrow x} = 1$ . (d)–(f) Same as (a)–(c), but here for the fractions of rejections of  $H_0^{\text{uni}}$  ( $\mathcal{V}_{x,1}$ ,  $\mathcal{M}_{x,1}$ , and  $\mathcal{S}_{x,1}$ ).

we have bidirectional coupling with unequal strengths ( $2 = \epsilon_{x \rightarrow y} > \epsilon_{y \rightarrow x} = 1$ ), noise  $\xi_y$  affects  $V_x$  to a lower degree. For the phase velocity standard deviation  $S_x$  [Fig. 4(c)], the noise dependence is similar to the one obtained for  $V_x$ . In Fig. 4(b), values of mean phase velocity  $M_x$  increase with higher values of  $\xi_x$ . To a lesser degree,  $M_x$  decreases for higher values of  $\xi_y$  most prominently at both high and low values of  $\xi_x$ . In general, lower counts of rejections ( $\mathcal{V}_{x,1}$ ,  $\mathcal{M}_{x,1}$ , and  $\mathcal{S}_{x,1}$ ) are found for those ranges of the noise  $\xi_{x,y}$  which lead to high values of the measures [Figs. 4(d)–4(f)].

### C. EEG signals from Bern-Barcelona database

We apply the univariate phase-based tests ( $\mathcal{V}$ ,  $\mathcal{M}$ , and  $\mathcal{S}$ ) and the bivariate phase-based test ( $\mathcal{R}$ ) to the 3750 focal and the 3750 nonfocal EEG signals constituting the Bern-Barcelona database. Recall that the database contains pairs of signals  $x$  and  $y$ , and for the univariate phase-based tests we only use signal  $x$ . In Fig. 5 we show the distributions of the values for the coefficient of phase velocity variation  $V$ , mean phase velocity  $M$ , phase velocity standard deviation  $S$ , and mean phase coherence  $R$  for both types of signals. Values of  $V$  have a higher mean and lower variability for focal signals [Fig. 5(a)] as compared to nonfocal signals [Fig. 5(e)]. For  $M$  values, focal signals have lower values on average [Fig. 5(b)] as compared to nonfocal signals [Fig. 5(f)]. Moreover, nonfocal signals have a more flat distribution with a not clear peak. With regard to  $S$ , we find on average higher values for nonfo-

cal signals [Fig. 5(g)] as compared to focal signals [Fig. 5(c)]. For the bivariate phase-based test we apply the mean phase coherence  $R$  to pairs of signals  $x$  and  $y$  from the database. We get higher values of  $R$  for focal signals on average [Fig. 5(d)] than for nonfocal signals [Fig. 5(h)]. Moreover, for nonfocal signals, the distribution of  $R$  is bimodal with a prominent peak for values close to 1.

In Fig. 5 we show the frequency of null hypothesis rejections of each phase-based test on dependence of the values of the underlying measures. Since the univariate tests reject  $H_0^{\text{uni}}$  if the measures' value for the original signal is lower than the minimum from the set of surrogates, we get more rejections in the left parts of the distributions. Using the mean phase velocity test  $\mathcal{M}$  we get the highest contrast between focal and nonfocal signals with regard to the frequency of  $H_0^{\text{uni}}$  rejections. A similar situation is obtained for the phase standard deviation test  $\mathcal{S}$ , although for this measure we have more rejections in nonfocal signals as compared to  $\mathcal{M}$ . Finally, using the coefficient of phase velocity variation test  $\mathcal{V}$  the frequency of null hypothesis rejections is similar for both groups of signals. As a consequence of these results, from the univariate tests we select the mean phase velocity test  $\mathcal{M}$  for the subsequent analysis. Regarding the bivariate mean phase coherence test  $\mathcal{R}$  we get a higher number of  $H_0^{\text{bi}}$  rejections in the middle and right parts of the distributions. This is because the bivariate test is rejected if the measures' value for the original pair of signals is higher than the maximum from the surrogates. As compared to the results for the univariate

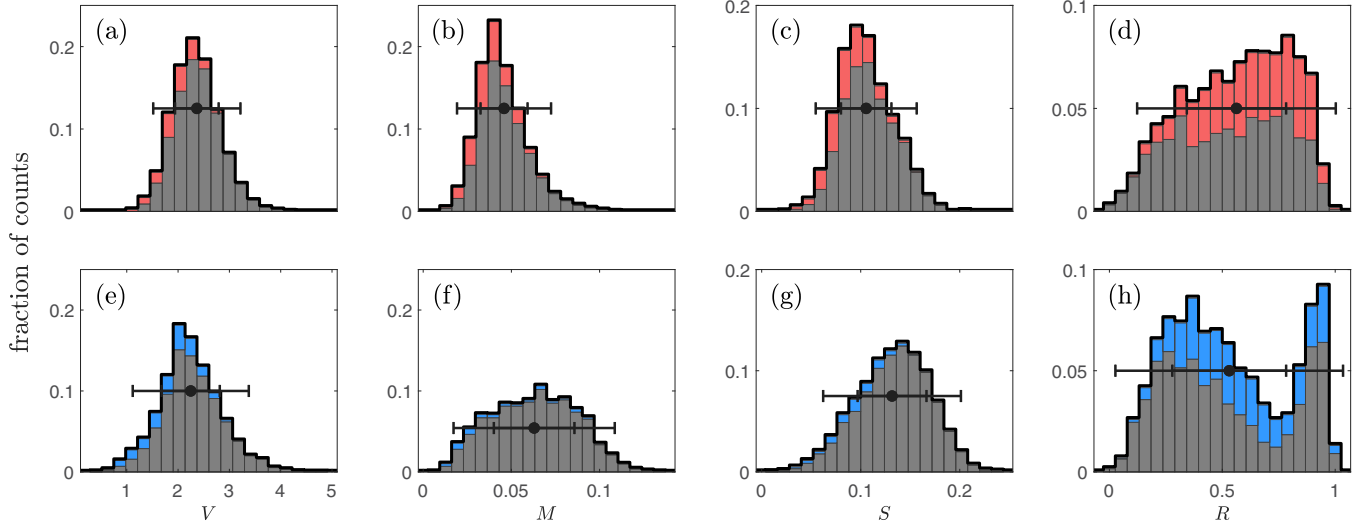


FIG. 5. Lower phase velocity and higher phase coherence is found for focal signals. Values for coefficient of phase velocity variation  $V$ , mean phase velocity  $M$ , phase velocity standard deviation  $S$ , and mean phase coherence  $R$  for (a)–(d) focal signals and (e)–(h) nonfocal signals. Normalized distributions are shown in black, and error bars represent mean values and two standard deviations. The grey parts of the stacked bars depict the subfraction of counts for which the null hypotheses are not rejected for each test ( $\mathcal{V}$ ,  $\mathcal{M}$ ,  $\mathcal{S}$ , and  $\mathcal{R}$ ). For the red and blue subfractions, the null hypotheses are rejected.

phase-based measures, here we get overall more rejections in both focal and nonfocal signals. However, the contrast between these two groups seems low.

We now quantify this contrast between the frequencies with which the null hypothesis is rejected for focal and nonfocal signals. Using the fractions of rejections for the mean phase velocity test for focal ( $\mathcal{M}_{f,1}$ ) and nonfocal signals ( $\mathcal{M}_{n,1}$ ) we define the relative difference  $\lambda_M$ :

$$\lambda_M = \frac{\mathcal{M}_{f,1} - \mathcal{M}_{n,1}}{\mathcal{M}_{f,1} + \mathcal{M}_{n,1}}. \quad (12)$$

Analogously, we define the relative difference  $\lambda_R$  for the mean phase coherence test:

$$\lambda_R = \frac{\mathcal{R}_{f,1} - \mathcal{R}_{n,1}}{\mathcal{R}_{f,1} + \mathcal{R}_{n,1}}. \quad (13)$$

The values of  $\lambda_M$  and  $\lambda_R$  are bounded in  $[-1, 1]$ , and we get positive values when the frequency of rejections for focal signals is higher than the one for nonfocal signals. Figure 6 shows the fraction of rejections for the phase-based tests  $\mathcal{M}$  and  $\mathcal{R}$  for both groups of signals and their respective relative differences  $\lambda_M$  and  $\lambda_R$ . The fraction  $\mathcal{M}_{n,1}$  is close to the chance level of 5%, whereas the other fractions are above. For both tests we obtain higher fractions of rejections for focal signals compared to nonfocal signals, resulting in  $\lambda_M > 0$  and  $\lambda_R > 0$ , where we get a higher contrast for the former ( $\lambda_M > \lambda_R$ ).

The EEG is a broadband signal and therefore its phase is not well defined using the Hilbert transform. A possible solution is to filter the EEG signal prior to the extraction of the phase [89]. To study this aspect, we bandpass filter the signals in the ranges of the classical EEG frequency bands:  $\delta$ ,  $\theta$ ,  $\alpha$ , and  $\beta$ . Figure 7 depicts the fractions of rejections for the phase-based tests  $\mathcal{M}$  and  $\mathcal{R}$  for these different frequency bands. In general,  $\mathcal{M}_{f,1}$  has decreased and in consequence also  $\lambda_M$  gets lower values as compared to Fig. 6. Therefore,

the prefiltering actually decreases the contrast between the focal and nonfocal signals. For the mean phase coherence test  $\mathcal{R}$  a different picture is obtained for the  $\alpha$  band and  $\beta$  band where higher values of  $\lambda_R$  are obtained. This analysis was also

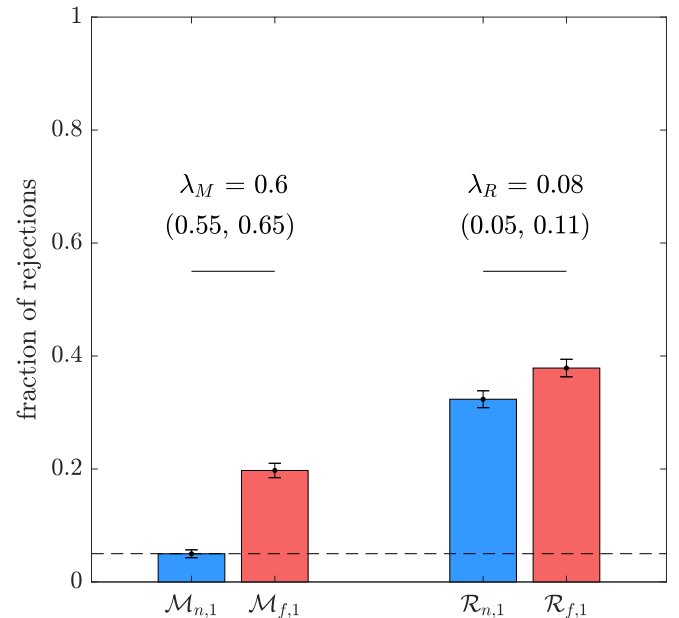


FIG. 6. The mean phase velocity test  $\mathcal{M}$  gives the higher contrast between focal and nonfocal signals. Rejection fractions for nonfocal (blue) and focal signals (red) for the mean phase velocity test  $\mathcal{M}$  and the mean phase coherence test  $\mathcal{R}$ . By construction the bar representing  $\mathcal{M}_{n,1}$  corresponds to the sum of all blue subfractions in Fig. 5(f), and analogously for the other quantities. The  $\lambda_M$  and  $\lambda_R$  values represent the relative difference for every pair of rejection fractions. The dashed line represents the significance level of the tests. The error bars and the numbers in brackets correspond to the 95% confidence interval (see Ref. [39]).

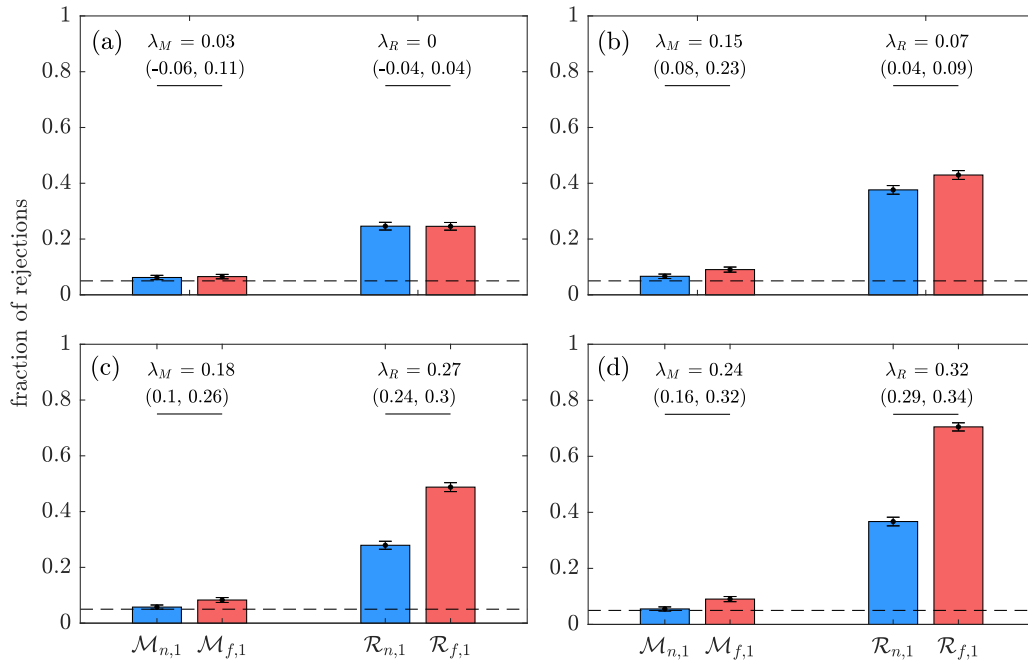


FIG. 7. Relative difference  $\lambda_M$  decreases while  $\lambda_R$  partly increases after prefiltering to different frequency bands. Same as Fig. 6 but after prefiltering using the frequency bands (a)  $\delta$  (0.5–4 Hz), (b)  $\theta$  (4–8 Hz), (c)  $\alpha$  (8–12 Hz), and (d)  $\beta$  (12–31 Hz).

performed using a bandpass filter in ranges of 2 Hz and they lead to qualitatively similar results as shown in Fig. 7 (results not shown).

#### IV. DISCUSSION

In this study we use univariate and bivariate phase-based measures to detect different features of EEG signals from epilepsy patients. We here present the univariate coefficient of phase velocity variation  $V$  based on the relative variability of instantaneous phase velocities to quantify phase irregularities from times series. This is done by dividing the phase velocity standard deviation  $S$  by its mean  $M$ . To the best of our knowledge, there are no studies applied to EEG signals from epilepsy patients analyzing phase irregularity measures. In agreement with previous studies [38] using bivariate measures, we find that focal signal pairs are more phase coherent than nonfocal signals as assessed by the mean phase coherence  $R$ . Furthermore, focal signals are less phase variable in absolute terms (phase velocity standard deviation  $S$ ) but more in relative terms (coefficient of phase velocity variation  $V$ ). Moreover, focal signals have lower mean phase velocity as assessed by  $M$ . When combined with surrogates, using the measures  $S$ ,  $M$ , and  $R$  for the phase-based tests we get more null hypothesis rejections for focal signals as compared to nonfocal signals. In particular, the measure  $M$  gives the highest contrast between focal and nonfocal signals. Therefore, focal signals are less consistent with the null hypotheses of univariate and bivariate surrogates than nonfocal signals. Furthermore, under controlled conditions based on Rössler dynamics, the measure  $M$  showed the highest sensitivity for features not included in  $H_0^{\text{uni}}$ .

We now compare our results with those from previous studies based on the Bern-Barcelona EEG database. Andrzejak *et al.* determined contrast values  $\lambda$  analogously to Eqs. (12) and (13) but based on a randomness test, a nonlinear-independence test, and a stationarity test [39]. They obtained  $\lambda$  values of 0.19, 0.15, and  $-0.09$ , respectively. Naro and colleagues applied a randomness test based on a novel rank-based nonlinear predictability score [43]. However, the authors did not specify the resulting  $\lambda$  value in Ref. [43]. Nonetheless, the authors of both Ref. [39] and Ref. [43] made the results for each signal publicly available at Refs. [49,121]. Thanks to this availability of the detailed results, we can compute the  $\lambda = 0.21$  value from Naro *et al.* without the necessity of recomputing the results for each signal using the source code available as well at Ref. [49]. Accordingly, our value of  $\lambda = 0.6$  obtained from the mean phase velocity test  $\mathcal{M}$  outperforms the results obtained in previous work. To further sustain this policy of open science, we provide our source codes and detailed results in the public domain [49,122].

For the interpretation of our results shown in Figs. 4–7, it is important to keep in mind that the outcome of any surrogate test cannot prove the nature of the underlying dynamics (see Ref. [39] and references therein). The specific null hypotheses  $H_0^{\text{uni}}$  and  $H_0^{\text{bi}}$  used here are composed by different assumptions about the dynamics. To test these hypotheses the randomization process performed to construct the surrogates destroys any nonlinear deterministic, any nonlinear interdependence and nonstationarity present in the original signals. Therefore, from a rejection of the null hypothesis  $H_0^{\text{uni}}$ , for example, one cannot conclude nonstochastic phase irregularity. That is because the null hypothesis could well be rejected because the dynamics are nonstationary. In Ref. [39] Andrzejak and colleagues used different conditioned surrogate tests to arrive at more specific conclusions about the dynamics underlying the

signals. Nonetheless, even combining the results of Ref. [39], using other kinds of surrogates (see Ref. [51]) and the results presented here, it remains impossible to understand totally the nature of the dynamics. Other types of surrogates, such as twin surrogates [123], can be applied for the study of brain dynamics [124].

It is also important to recall that one cannot conclude from the mean phase coherence obtained for a pair of signals to a coupling between different brain areas from which the signals were measured. A common driving from an unmeasured source is only one of several possible reasons that would impede such a conclusion. This limitation is also not overcome by using surrogates, which only help to reduce the influence of linear correlations and non-Gaussianity in the amplitudes. A detection of causal interactions in human epilepsy networks requires much more elaborate approaches (see for example Refs. [125,126]). The key point is that we do not aim at detecting a coupling or even estimating a coupling strength. We only compare the mean phase coherence and our other measures as well as the rejection rates of the corresponding surrogate tests obtained for focal versus nonfocal signal pairs. Any type of bias unrelated to epilepsy can be expected to affect the results obtained for focal and nonfocal signal pairs in the same way. Accordingly, the contrasts we find between these two signal classes can be attributed to the impact that epilepsy has on the EEG signal during the seizure-free interval.

The Bern-Barcelona EEG database which we analyzed in this study contains only relatively short EEG signal pairs cut from recordings performed during the seizure-free interval. Future work should analyze long-term multichannel EEG recordings also including epileptic seizures. Seizures are not a steady-state dynamics. Both the EEG frequency content (e.g., Ref. [127]) and the degree of synchronization (e.g., Refs. [128,129]) show a complex temporal evolution across the duration of the seizure. This calls for the application of time-resolved measures to optimally capture evolving seizure dynamics. Prior to applying an interaction measure such as the mean phase coherence to sources reconstructed from scalp EEG or magnetoencephalographic (MEG) data with the aim to study long-range interactions among cortical processes, spurious correlations caused by instantaneous field spread and volume conduction must be carefully considered [130].

For the results shown in Figs. 3 and 4, we work under controlled conditions applying dynamical noise to two non-identical coupled Rössler dynamics for different symmetric and asymmetric coupling schemes. For unidirectional coupling and intermediate noise levels we obtain high levels of mean phase coherence  $R$  and low values of the coefficient of phase velocity variation  $V$ . This means that under certain conditions noise can help both systems to synchronize and reduce phase irregularities. Accordingly, we observe results resembling stochastic resonance in both phase-based measures. This consistency between the two measures under controlled con-

ditions further supports that the coefficient of phase velocity variation  $V$  allows for a meaningful characterization of the dynamics underlying experimental signals.

We extract the phase from observable data using the Hilbert transform, and some studies consider it as a not well-defined phase because it might not evolve uniformly in time [88]. Therefore, in Ref. [88] this phase extracted from the Hilbert transform is used only as a preliminary variable to then obtain a genuine phase. However, this genuine phase is defined for limit-cycle oscillators [88] and is therefore not applicable to the dynamics we study here. In any case, a better defined phase can be obtained by filtering the signal to narrow frequency bands. Therefore, in order to study the influence of prefiltering, we select the classical frequency bands  $\delta$ ,  $\theta$ ,  $\alpha$ , and  $\beta$  and bands with a width of 2 Hz. We find that the performance of the univariate test decreases due to the filtering. It is important also to note that while filtering generally facilitates the extraction of a phase, it relies on the assumption that the dynamics can be fully decomposed into narrow-band oscillations. However, this assumption does not account for the presence of aperiodic components in neural power spectra (see, for example, Refs. [131–133]). This consideration and the decreased performance of the univariate tests for filtered data reinforce our approach to deliberately use the phase extracted from unfiltered broadband signals directly by means of the Hilbert transform. It is this approach which allows us to characterize any possible deviation from the strictly linear phase growth, such as nonlinearity, nonstationarity, chaoticity, and noise. In contrast, for the bivariate test the performance increases for certain frequency bands showing that in order to assess phase synchronization narrow-band signals are more suited.

The phase-based measures are conceptually simple and easy to compute and this can help when analyzing big databases. Despite this simplicity they give relevant information about the underlying dynamics of focal and nonfocal EEG signals from epilepsy patients. Even in the absence of seizures we can detect different features induced by epilepsy. We compare different univariate and bivariate phase-based measures under controlled conditions. The univariate measure mean phase velocity gives the highest sensitivity in a surrogate test. This is translated to a high contrast between focal and nonfocal signals in the rejections of the surrogates' null hypotheses. From a clinical point of view, the simplicity of the definition and computation of our phase-based measures can be useful in the presurgical evaluation of epilepsy.

#### ACKNOWLEDGMENTS

This project was supported by the Spanish Ministry of Science and Innovation and the State Research Agency (Grant No. PID2020-118196GB-I00/MICIN/AEI/10.13039/501100011033).

[1] R. S. Fisher, C. Acevedo, A. Arzimanoglou, A. Bogacz, J. H. Cross, C. E. Elger, J. Engel, Jr., L. Forsgren, J. A. French, M. Glynn *et al.*, ILAE official report: A practical clinical definition of epilepsy, *Epilepsia* **55**, 475 (2014).

[2] F. Rosenow and H. Lüders, Presurgical evaluation of epilepsy, *Brain* **124**, 1683 (2001).

[3] H. O. Lüders, I. Najm, D. Nair, P. Widdess-Walsh, and W. Bingman, The epileptogenic zone: General principles, *Epileptic Disord.* **8**, S1-9 (2006).

- [4] V. N. Vakharia, J. S. Duncan, J. A. Witt, C. E. Elger, R. Staba, and J. Engel, Jr., Getting the best outcomes from epilepsy surgery, *Ann. Neurol.* **83**, 676 (2018).
- [5] J. Yuan, Y. Chen, and E. Hirsch, Intracranial electrodes in the presurgical evaluation of epilepsy, *Neurol. Sci.* **33**, 723 (2012).
- [6] A. Korzeniewska, M. C. Cervenka, C. C. Jouny, J. R. Perilla, J. Harezlak, G. K. Bergey, P. J. Franaszczuk, and N. E. Crone, Ictal propagation of high frequency activity is recapitulated in interictal recordings: Effective connectivity of epileptogenic networks recorded with intracranial EEG, *NeuroImage* **101**, 96 (2014).
- [7] K. A. G. Otárola, Y. Mikhaeil-Demo, E. M. Bachman, P. Balaguera, and S. Schuele, Automated seizure detection accuracy for ambulatory EEG recordings, *Neurology* **92**, e1540 (2019).
- [8] M. C. Casdagli, L. D. Iasemidis, R. S. Savit, R. L. Gilmore, S. N. Roper, and J. C. Sackellares, Non-linearity in invasive EEG recordings from patients with temporal lobe epilepsy, *Electroencephalogr. Clin. Neurophysiol.* **102**, 98 (1997).
- [9] R. G. Andrzejak, K. Lehnertz, F. Mormann, C. Rieke, P. David, and C. E. Elger, Indications of nonlinear deterministic and finite-dimensional structures in time series of brain electrical activity: Dependence on recording region and brain state, *Phys. Rev. E* **64**, 061907 (2001).
- [10] P. Van Mierlo, E. Carrette, H. Hallez, R. Raedt, A. Meurs, S. Vandenberghe, D. Van Roost, P. Boon, S. Staelens, and K. Vonck, Ictal-onset localization through connectivity analysis of intracranial EEG signals in patients with refractory epilepsy, *Epilepsia* **54**, 1409 (2013).
- [11] V. Gnatkovsky, S. Francione, F. Cardinale, R. Mai, L. Tassi, G. Lo Russo, and M. De Curtis, Identification of reproducible ictal patterns based on quantified frequency analysis of intracranial EEG signals, *Epilepsia* **52**, 477 (2011).
- [12] K. Schindler, C. Rummel, R. G. Andrzejak, M. Goodfellow, F. Zubler, E. Abela, R. Wiest, C. Pollo, A. Steimer, and H. Gast, Ictal time-irreversible intracranial EEG signals as markers of the epileptogenic zone, *Clin. Neurophysiol.* **127**, 3051 (2016).
- [13] P. J. Franaszczuk and G. K. Bergey, An autoregressive method for the measurement of synchronization of interictal and ictal EEG signals, *Biol. Cybern.* **81**, 3 (1999).
- [14] R. B. Pachori, Discrimination between ictal and seizure-free EEG signals using empirical mode decomposition, *Res. Lett. Signal Process.* **2008**, 293056 (2008).
- [15] R. B. Duckrow and S. S. Spencer, Regional coherence and the transfer of ictal activity during seizure onset in the medial temporal lobe, *Electroencephalogr. Clin. Neurophysiol.* **82**, 415 (1992).
- [16] M. Van der Heyden, D. Velis, B. Hoekstra, J. Pijn, W. van Emde Boas, C. Van Veelen, P. Van Rijen, F. L. da Silva, and J. DeGoede, Non-linear analysis of intracranial human EEG in temporal lobe epilepsy, *Clin. Neurophysiol.* **110**, 1726 (1999).
- [17] M. G. Leguia, C. G. B. Martínez, I. Malvestio, A. T. Campo, R. Rocamora, Z. Levnajić, and R. G. Andrzejak, Inferring directed networks using a rank-based connectivity measure, *Phys. Rev. E* **99**, 012319 (2019).
- [18] M. Le Van Quyen, C. Adam, M. Baulac, J. Martinerie, and F. J. Varela, Nonlinear interdependencies of EEG signals in human intracranially recorded temporal lobe seizures, *Brain Res.* **792**, 24 (1998).
- [19] C. Rummel, R. G. Andrzejak, and K. Schindler, Quantitative analysis of peri-ictal multi-channel EEG, *Epileptologie* **113**, 29 (2012).
- [20] K. Schindler, H. Gast, M. Goodfellow, and C. Rummel, On seeing the trees and the forest: Single-signal and multisignal analysis of periictal intracranial EEG, *Epilepsia* **53**, 1658 (2012).
- [21] M. Müller, M. Caporro, H. Gast, C. Pollo, R. Wiest, K. Schindler, and C. Rummel, Linear and nonlinear interrelations show fundamentally distinct network structure in preictal intracranial EEG of epilepsy patients, *Human Brain Mapping* **41**, 467 (2020).
- [22] G. Varotto, L. Tassi, S. Franceschetti, R. Spreafico, and F. Panzica, Epileptogenic networks of type II focal cortical dysplasia: A stereo-EEG study, *NeuroImage* **61**, 591 (2012).
- [23] R. G. Andrzejak, D. Chicharro, K. Lehnertz, and F. Mormann, Using bivariate signal analysis to characterize the epileptic focus: The benefit of surrogates, *Phys. Rev. E* **83**, 046203 (2011).
- [24] C. G. Martínez, J. Niediek, F. Mormann, and R. G. Andrzejak, Seizure onset zone lateralization using a non-linear analysis of micro vs. macro electroencephalographic recordings during seizure-free stages of the sleep-wake cycle from epilepsy patients, *Front. Neurol.* **11**, 1057 (2020).
- [25] M. Marciani, F. Stefanini, N. Stefani, M. Maschio, G. Gigli, S. Roncacci, C. Caltagirone, and G. Bernardi, Lateralization of the epileptogenic focus by computerized EEG study and neuropsychological evaluation, *Int. J. Neurosci.* **66**, 53 (1992).
- [26] D. Panet-Raymond and J. Gotman, Asymmetry in delta activity in patients with focal epilepsy, *Electroencephalogr. Clin. Neurophysiol.* **75**, 474 (1990).
- [27] M. E. Drake, H. Padamadan, and S. A. Newell, Interictal quantitative EEG in epilepsy, *Seizure* **7**, 39 (1998).
- [28] J. Wang and H. G. Wieser, Regional “rigidity” of background EEG activity in the epileptogenic zone, *Epilepsia* **35**, 495 (1994).
- [29] A. Tuunainen, U. Nousiainen, A. Pilke, E. Mervaala, J. Partanen, and P. Riekkinen, Spectral EEG during short-term discontinuation of antiepileptic medication in partial epilepsy, *Epilepsia* **36**, 817 (1995).
- [30] C. P. Warren, S. Hu, M. Stead, B. H. Brinkmann, M. R. Bower, and G. A. Worrell, Synchrony in normal and focal epileptic brain: The seizure onset zone is functionally disconnected, *J. Neurophysiol.* **104**, 3530 (2010).
- [31] H. Osterhage, F. Mormann, M. Staniek, and K. Lehnertz, Measuring synchronization in the epileptic brain: A comparison of different approaches, *Int. J. Bifurcation Chaos* **17**, 3539 (2007).
- [32] G. J. Ortega, L. Menendez de la Prida, R. G. Sola, and J. Pastor, Synchronization clusters of interictal activity in the lateral temporal cortex of epileptic patients: Intraoperative electrocorticographic analysis, *Epilepsia* **49**, 269 (2008).
- [33] E. H. Park and J. R. Madsen, Granger causality analysis of interictal iEEG predicts seizure focus and ultimate resection, *Neurosurgery* **82**, 99 (2018).
- [34] J. Dauwels, E. Eskandar, and S. Cash, Localization of seizure onset area from intracranial non-seizure EEG by exploiting locally enhanced synchrony, in *2009 Annual International Conference of the IEEE Engineering in Medicine and Biology Society* (IEEE, New York, 2009), pp. 2180–2183.

- [35] S. Meesters, P. Ossenblok, A. Colon, L. Wagner, O. Schijns, P. Boon, L. Florack, and A. Fuster, Modeling of intracerebral interictal epileptic discharges: Evidence for network interactions, *Clin. Neurophysiol.* **129**, 1276 (2018).
- [36] G. Bettus, F. Wendling, M. Guye, L. Valton, J. Régis, P. Chauvel, and F. Bartolomei, Enhanced EEG functional connectivity in mesial temporal lobe epilepsy, *Epilepsy Res.* **81**, 58 (2008).
- [37] C. A. Schevon, J. Cappell, R. Emerson, J. Isler, P. Grieve, R. Goodman, G. Mckhann, Jr., H. Weiner, W. Doyle, R. Kuzniecky *et al.*, Cortical abnormalities in epilepsy revealed by local EEG synchrony, *NeuroImage* **35**, 140 (2007).
- [38] F. Mormann, K. Lehnertz, P. David, and C. E. Elger, Mean phase coherence as a measure for phase synchronization and its application to the EEG of epilepsy patients, *Physica D* **144**, 358 (2000).
- [39] R. G. Andrzejak, K. Schindler, and C. Rummel, Non-randomness, nonlinear dependence, and nonstationarity of electroencephalographic recordings from epilepsy patients, *Phys. Rev. E* **86**, 046206 (2012).
- [40] J. Arnhold, P. Grassberger, K. Lehnertz, and C. E. Elger, A robust method for detecting interdependences: Application to intracranially recorded EEG, *Physica D* **134**, 419 (1999).
- [41] M. Le Van Quyen, J. Martinerie, C. Adam, and F. J. Varela, Nonlinear analyses of interictal EEG map the brain interdependences in human focal epilepsy, *Physica D* **127**, 250 (1999).
- [42] M. Staniak and K. Lehnertz, Symbolic Transfer Entropy, *Phys. Rev. Lett.* **100**, 158101 (2008).
- [43] D. Naro, C. Rummel, K. Schindler, and R. G. Andrzejak, Detecting determinism with improved sensitivity in time series: Rank-based nonlinear predictability score, *Phys. Rev. E* **90**, 032913 (2014).
- [44] R. G. Andrzejak, F. Mormann, G. Widman, T. Kreuz, C. E. Elger, and K. Lehnertz, Improved spatial characterization of the epileptic brain by focusing on nonlinearity, *Epilepsy Res.* **69**, 30 (2006).
- [45] R. G. Andrzejak, G. Widman, K. Lehnertz, C. Rieke, P. David, and C. Elger, The epileptic process as nonlinear deterministic dynamics in a stochastic environment: An evaluation on mesial temporal lobe epilepsy, *Epilepsy Res.* **44**, 129 (2001).
- [46] K. Lehnertz and C. Elger, Spatio-temporal dynamics of the primary epileptogenic area in temporal lobe epilepsy characterized by neuronal complexity loss, *Electroencephalogr. Clin. Neurophysiol.* **95**, 108 (1995).
- [47] M. Carreno and H. O. Lüders, General principles of pre-surgical evaluation, in *Textbook of Epilepsy Surgery* (CRC Press, Boca Raton, FL, 2008), pp. 449–464.
- [48] X. Setoain, M. Carreño, J. Pavía, B. Martí-Fuster, F. Campos, and F. Lomeña, PET and SPECT in epilepsy, *Rev. Esp. Med. Nucl. Imagen Mol. (Engl. Ed.)* **33**, 165 (2014).
- [49] R. G. Andrzejak, K. Schindler, and C. Rummel, Bern-Barcelona database (2012), <https://www.upf.edu/web/ntsa/downloads>.
- [50] J. Theiler, S. Eubank, A. Longtin, B. Galdrikian, and J. D. Farmer, Testing for nonlinearity in time series: The method of surrogate data, *Physica D* **58**, 77 (1992).
- [51] N. P. Subramaniam and J. Hyttinen, Dynamics of intracranial electroencephalographic recordings from epilepsy patients using univariate and bivariate recurrence networks, *Phys. Rev. E* **91**, 022927 (2015).
- [52] R. Sharma, R. B. Pachori, and U. R. Acharya, Application of entropy measures on intrinsic mode functions for the automated identification of focal electroencephalogram signals, *Entropy* **17**, 669 (2015).
- [53] R. Sharma, R. B. Pachori, and U. R. Acharya, An integrated index for the identification of focal electroencephalogram signals using discrete wavelet transform and entropy measures, *Entropy* **17**, 5218 (2015).
- [54] M. Sharma, A. Dhere, R. B. Pachori, and U. R. Acharya, An automatic detection of focal EEG signals using new class of time–frequency localized orthogonal wavelet filter banks, *Knowl.-Based Syst.* **118**, 217 (2017).
- [55] U. R. Acharya, Y. Hagiwara, S. N. Deshpande, S. Suren, J. E. W. Koh, S. L. Oh, N. Arunkumar, E. J. Ciaccio, and C. M. Lim, Characterization of focal EEG signals: A review, *Future Gener. Comput. Syst.* **91**, 290 (2019).
- [56] T. Zhang, Z. Han, X. Chen, and W. Chen, Quantifying randomness and complexity of a signal via maximum fuzzy membership difference entropy, *Measurement* **174**, 109053 (2021).
- [57] A. Mirzaei, A. Ayatollahi, and H. Vavadi, Statistical analysis of epileptic activities based on histogram and wavelet-spectral entropy, *J. Biomed. Sci. Eng.* **4**, 207 (2011).
- [58] Y. Kumar, M. Dewal, and R. Anand, Features extraction of EEG signals using approximate and sample entropy, in *2012 IEEE Students' Conference on Electrical, Electronics and Computer Science* (IEEE, New York, 2012), pp. 1–5.
- [59] L. C. Amarantidis and D. Abásolo, Interpretation of entropy algorithms in the context of biomedical signal analysis and their application to EEG analysis in epilepsy, *Entropy* **21**, 840 (2019).
- [60] H. Vavadi, A. Ayatollahi, and A. Mirzaei, A wavelet-approximate entropy method for epileptic activity detection from EEG and its sub-bands, *J. Biomed. Sci. Eng.* **3**, 1182 (2010).
- [61] A. Kraskov, Synchronization and interdependence measures and their applications to the electroencephalogram of epilepsy patients and clustering of data, Ph.D. thesis, Universität Wuppertal, Fakultät für Mathematik und Naturwissenschaften (2004).
- [62] C. G. Martínez, Nonlinear signal analysis of micro and macro electroencephalographic recordings from epilepsy patients, Ph.D. thesis, Universitat Pompeu Fabra (2020).
- [63] T. Inouye, K. Shinosaki, H. Sakamoto, S. Toi, S. Ukai, A. Iyama, Y. Katsuda, and M. Hirano, Quantification of EEG irregularity by use of the entropy of the power spectrum, *Electroencephalogr. Clin. Neurophysiol.* **79**, 204 (1991).
- [64] H. Azami, D. Abásolo, S. Simons, and J. Escudero, Univariate and multivariate generalized multiscale entropy to characterise EEG signals in Alzheimer's disease, *Entropy* **19**, 31 (2017).
- [65] D. Abásolo, R. Hornero, P. Espino, D. Alvarez, and J. Poza, Entropy analysis of the EEG background activity in Alzheimer's disease patients, *Physiol. Meas.* **27**, 241 (2006).
- [66] P. Vijayakumaran, D. Narzary, V. Gonuguntla, H. W. Lee, and K. C. Veluvolu, EEG based functional connectivity analysis of Alzheimer's disease subjects, in *2020 International Conference on Artificial Intelligence in Information and Communication (ICAIIIC)* (IEEE, New York, 2020), pp. 356–361.

- [67] S. M. Pincus, Approximate entropy as a measure of irregularity for psychiatric serial metrics, *Bipolar Disord.* **8**, 430 (2006).
- [68] H. Sohn, I. Kim, W. Lee, B. S. Peterson, H. Hong, J. H. Chae, S. Hong, and J. Jeong, Linear and non-linear EEG analysis of adolescents with attention-deficit/hyperactivity disorder during a cognitive task, *Clin. Neurophysiol.* **121**, 1863 (2010).
- [69] F. Zappasodi, E. Olejarczyk, L. Marzetti, G. Assenza, V. Pizzella, and F. Tecchio, Fractal dimension of EEG activity senses neuronal impairment in acute stroke, *PLoS One* **9**, e100199 (2014).
- [70] J. Kim, J. H. Chae, H. K. Ko, C. F. V. Latchoumane, A. Banerjee, D. J. Mandell, C. W. Hoven, and J. Jeong, Hemispheric asymmetry in non-linear interdependence of EEG in post-traumatic stress disorder, *Psychiatry Clin. Neurosci.* **66**, 87 (2012).
- [71] J. Dauwels, F. Vialatte, T. Musha, and A. Cichocki, A comparative study of synchrony measures for the early diagnosis of Alzheimer's disease based on EEG, *NeuroImage* **49**, 668 (2010).
- [72] J. Jeong, EEG dynamics in patients with Alzheimer's disease, *Clin. Neurophysiol.* **115**, 1490 (2004).
- [73] X. Guo, W. Wu, and S. Tong, Asymmetry of hemispheric interdependences in the early hours following unilateral stroke: An electrophysiological study in rats, in *2017 39th Annual International Conference of the IEEE Engineering in Medicine and Biology Society (EMBC)* (IEEE, New York, 2017), pp. 4363–4366.
- [74] A. Galka, *Topics in Nonlinear Time Series Analysis: With Implications for EEG Analysis* (World Scientific, Singapore, 2000), Vol. 14.
- [75] F. Karimzadeh, R. Boostani, E. Seraj, and R. Sameni, A distributed classification procedure for automatic sleep stage scoring based on instantaneous electroencephalogram phase and envelope features, *IEEE Trans. Neural Syst. Rehabil. Eng.* **26**, 362 (2017).
- [76] P. Bob, M. Palus, M. Susta, and K. Glaslova, EEG phase synchronization in patients with paranoid schizophrenia, *Neurosci. Lett.* **447**, 73 (2008).
- [77] M. Le Van Quyen, J. Foucher, J. P. Lachaux, E. Rodriguez, A. Lutz, J. Martinerie, and F. J. Varela, Comparison of Hilbert transform and wavelet methods for the analysis of neuronal synchrony, *J. Neurosci. Methods* **111**, 83 (2001).
- [78] V. V. Nikulin and T. Brismar, Phase synchronization between alpha and beta oscillations in the human electroencephalogram, *Neuroscience* **137**, 647 (2006).
- [79] G. Bortnyk, M. Vasylykivskiy, and V. Kychak, The method of improving the dynamic range of analog-digital conversion of phase jitter signals in telecommunications systems, in *2016 International Conference Radio Electronics & Info Communications (UkrMiCo)* (IEEE, New York, 2016), pp. 1–7.
- [80] J. Boiko, V. Tolubko, O. Barabash, O. Eromenko, and Y. Havrylko, Signal processing with frequency and phase shift keying modulation in telecommunications, *Telkomnika* **17**, 2025 (2019).
- [81] D. Benitez, P. Gaydecki, A. Zaidi, and A. Fitzpatrick, The use of the Hilbert transform in ECG signal analysis, *Comput. Biol. Med.* **31**, 399 (2001).
- [82] S. Mishra, D. Das, R. Kumar, and P. Sumathi, A power-line interference canceler based on sliding DFT phase locking scheme for ECG signals, *IEEE Trans. Instrum. Meas.* **64**, 132 (2014).
- [83] Y. Zheng, Y. Wang, and X. Chang, 3D forward modeling of upgoing and downgoing wavefields using Hilbert transform, *Geophysics* **83**, F1 (2018).
- [84] Y. Luo, S. Al-Dossary, M. Marhoon, and M. Alfaraj, Generalized Hilbert transform and its applications in geophysics, *Leading Edge* **22**, 198 (2003).
- [85] D. Gabor, Theory of communication. Part 1: The analysis of information, *J. Inst. Electr. Eng.* **93**, 429 (1946).
- [86] A. Grossmann, R. Kronland-Martinet, and J. Morlet, Reading and understanding continuous wavelet transforms, in *Wavelets* (Springer, Berlin, 1990), pp. 2–20.
- [87] A. Pikovsky, M. Rosenblum, and J. Kurths, *Synchronization: A universal Concept in Nonlinear Sciences* (Cambridge University Press, Cambridge, UK, 2003), Vol. 12.
- [88] B. Kraleman, L. Cimponeriu, M. Rosenblum, A. Pikovsky, and R. Mrowka, Phase dynamics of coupled oscillators reconstructed from data, *Phys. Rev. E* **77**, 066205 (2008).
- [89] R. Q. Quiroga, A. Kraskov, T. Kreuz, and P. Grassberger, Performance of different synchronization measures in real data: A case study on electroencephalographic signals, *Phys. Rev. E* **65**, 041903 (2002).
- [90] J. T. Schwabedal, Parametric phase diffusion analysis of irregular oscillations, *Europhys. Lett.* **107**, 68001 (2014).
- [91] C. Schäfer, M. G. Rosenblum, J. Kurths, and H. H. Abel, Heartbeat synchronized with ventilation, *Nature (London)* **392**, 239 (1998).
- [92] R. Bartsch, J. W. Kantelhardt, T. Penzel, and S. Havlin, Experimental Evidence for Phase Synchronization Transitions in the Human Cardiorespiratory System, *Phys. Rev. Lett.* **98**, 054102 (2007).
- [93] A. Kuhnhold, A. Y. Schumann, R. P. Bartsch, R. Ubrich, P. Barthel, G. Schmidt, and J. W. Kantelhardt, Quantifying cardio-respiratory phase synchronization—a comparison of five methods using ECGs of post-infarction patients, *Physiol. Meas.* **38**, 925 (2017).
- [94] P. Tass, M. G. Rosenblum, J. Weule, J. Kurths, A. Pikovsky, J. Volkman, A. Schnitzler, and H. J. Freund, Detection of  $n : m$  Phase Locking from Noisy Data: Application to Magnetoencephalography, *Phys. Rev. Lett.* **81**, 3291 (1998).
- [95] S. Olbrich, A. Tränkner, T. Chittka, U. Hegerl, and P. Schönknecht, Functional connectivity in major depression: Increased phase synchronization between frontal cortical EEG-source estimates, *Psychiatry Res., Neuroimaging* **222**, 91 (2014).
- [96] D. Gupta and C. J. James, Narrowband vs. broadband phase synchronization analysis applied to independent components of ictal and interictal EEG, in *2007 29th Annual International Conference of the IEEE Engineering in Medicine and Biology Society* (IEEE, New York, 2007), pp. 3864–3867.
- [97] D. Rangaprakash and N. Pradhan, Study of phase synchronization in multichannel seizure EEG using nonlinear recurrence measure, *Biomed. Signal Process. Control* **11**, 114 (2014).
- [98] L. G. Dominguez, R. A. Wennberg, W. Gaetz, D. Cheyne, O. C. Snead, and J. L. P. Velazquez, Enhanced synchrony in epileptiform activity? Local versus distant phase synchronization in generalized seizures, *J. Neurosci.* **25**, 8077 (2005).

- [99] F. Mormann, T. Kreuz, R. G. Andrzejak, P. David, K. Lehnertz, and C. E. Elger, Epileptic seizures are preceded by a decrease in synchronization, *Epilepsy Res.* **53**, 173 (2003).
- [100] Y. Zheng, G. Wang, K. Li, G. Bao, and J. Wang, Epileptic seizure prediction using phase synchronization based on bivariate empirical mode decomposition, *Clin. Neurophysiol.* **125**, 1104 (2014).
- [101] L. Callenbach, P. Hänggi, S. J. Linz, J. A. Freund, and L. Schimansky-Geier, Oscillatory systems driven by noise: Frequency and phase synchronization, *Phys. Rev. E* **65**, 051110 (2002).
- [102] R. Follmann, E. Rosa, Jr., E. E. Macau, and J. R. C. Piqueira, Identifying phase synchronous regimes in non-coherent and multiple scroll attractor systems, *Int. J. Bifurcation Chaos* **23**, 1350179 (2013).
- [103] J. P. Lachaux, E. Rodriguez, J. Martinerie, and F. J. Varela, Measuring phase synchrony in brain signals, *Human Brain Mapping* **8**, 194 (1999).
- [104] P. S. Baboukani, G. Azemi, B. Boashash, P. Colditz, and A. Omidvarnia, A novel multivariate phase synchrony measure: Application to multichannel newborn EEG analysis, *Digital Signal Process.* **84**, 59 (2019).
- [105] V. Sakkalis, C. D. Giurcaneanu, P. Xanthopoulos, M. E. Zervakis, V. Tsiaras, Y. Yang, E. Karakonstantaki, and S. Micheloyannis, Assessment of linear and nonlinear synchronization measures for analyzing EEG in a mild epileptic paradigm, *IEEE Trans. Inf. Technol. Biomed.* **13**, 433 (2008).
- [106] N. P. Subramaniyam and J. Hyttinen, Characterization of dynamical systems under noise using recurrence networks: Application to simulated and EEG data, *Phys. Lett. A* **378**, 3464 (2014).
- [107] T. V. Yakovleva, I. E. Kutepov, A. Y. Karas, N. M. Yakovlev, V. V. Dobriyan, I. V. Papkova, M. V. Zhigalov, O. A. Saltykova, A. V. Krysko, T. Y. Yaroshenko *et al.*, EEG analysis in structural focal epilepsy using the methods of nonlinear dynamics (Lyapunov exponents, Lempel-Ziv complexity, and multiscale entropy), *Sci. World J.* **2020**, 8407872 (2020).
- [108] J. P. Pijn, J. Van Neerven, A. Noest, and F. H. L. da Silva, Chaos or noise in EEG signals; dependence on state and brain site, *Electroencephalogr. Clin. Neurophysiol.* **79**, 371 (1991).
- [109] O. E. Rössler, An equation for continuous chaos, *Phys. Lett. A* **57**, 397 (1976).
- [110] M. Rosenblum and J. Kurths, Analysing synchronization phenomena from bivariate data by means of the Hilbert transform, in *Nonlinear Analysis of Physiological Data* (Springer, Berlin, 1998), pp. 91–99.
- [111] M. T. Taner, F. Koehler, and R. Sheriff, Complex seismic trace analysis, *Geophysics* **44**, 1041 (1979).
- [112] T. E. Scheuer and D. W. Oldenburg, Local phase velocity from complex seismic data, *Geophysics* **53**, 1503 (1988).
- [113] M. X. Cohen, Fluctuations in oscillation frequency control spike timing and coordinate neural networks, *J. Neurosci.* **34**, 8988 (2014).
- [114] M. G. Rosenblum, A. S. Pikovsky, and J. Kurths, Phase Synchronization of Chaotic Oscillators, *Phys. Rev. Lett.* **76**, 1804 (1996).
- [115] T. Schreiber and A. Schmitz, Improved Surrogate Data for Nonlinearity Tests, *Phys. Rev. Lett.* **77**, 635 (1996).
- [116] D. Prichard and J. Theiler, Generating Surrogate Data for Time Series with Several Simultaneously Measured Variables, *Phys. Rev. Lett.* **73**, 951 (1994).
- [117] T. Schreiber and A. Schmitz, Surrogate time series, *Physica D* **142**, 346 (2000).
- [118] R. G. Andrzejak, A. Kraskov, H. Stögbauer, F. Mormann, and T. Kreuz, Bivariate surrogate techniques: Necessity, strengths, and caveats, *Phys. Rev. E* **68**, 066202 (2003).
- [119] A. Neiman, A. Silchenko, V. Anishchenko, and L. Schimansky-Geier, Stochastic resonance: Noise-enhanced phase coherence, *Phys. Rev. E* **58**, 7118 (1998).
- [120] L. Gammaitoni, P. Hänggi, P. Jung, and F. Marchesoni, Stochastic resonance, *Rev. Mod. Phys.* **70**, 223 (1998).
- [121] R. G. Andrzejak, K. Schindler, and C. Rummel, Bern-Barcelona database UPF library (2012), <http://hdl.handle.net/10230/42829>.
- [122] A. Espinosa and R. G. Andrzejak, GitHub repository source code and results (2022), [https://github.com/aespinoso/Espinosa\\_2022.git](https://github.com/aespinoso/Espinosa_2022.git).
- [123] M. Thiel, M. C. Romano, J. Kurths, M. Rolf, and R. Kliegl, Twin surrogates to test for complex synchronisation, *Europhys. Lett.* **75**, 535 (2006).
- [124] G. Lancaster, D. Iatsenko, A. Pidde, V. Ticcinelli, and A. Stefanovska, Surrogate data for hypothesis testing of physical systems, *Phys. Rep.* **748**, 1 (2018).
- [125] L. Faes, D. Marinazzo, and S. Stramaglia, Multiscale information decomposition: Exact computation for multivariate Gaussian processes, *Entropy* **19**, 408 (2017).
- [126] R. D. Pascual-Marqui, R. J. Biscay, J. Bosch-Bayard, P. Achermann, P. Faber, T. Kinoshita, and K. Kochi, Linear causal filtering: Definition and theory, *bioRxiv* (2021), doi: 10.1101/2021.05.01.442232.
- [127] S. J. Schiff, D. Colella, G. M. Jacyna, E. Hughes, J. W. Creekmore, A. Marshall, M. Bozek-Kuzmicki, G. Benke, W. D. Gaillard, J. Conry *et al.*, Brain chirps: Spectrographic signatures of epileptic seizures, *Clin. Neurophysiol.* **111**, 953 (2000).
- [128] P. Jiruska, M. De Curtis, J. G. Jefferys, C. A. Schevon, S. J. Schiff, and K. Schindler, Synchronization and desynchronization in epilepsy: Controversies and hypotheses, *J. Physiol.* **591**, 787 (2013).
- [129] K. Schindler, H. Leung, C. E. Elger, and K. Lehnertz, Assessing seizure dynamics by analysing the correlation structure of multichannel intracranial EEG, *Brain* **130**, 65 (2007).
- [130] J. M. Palva, S. H. Wang, S. Palva, A. Zhigalov, S. Monto, M. J. Brookes, J.-M. Schoffelen, and K. Jerbi, Ghost interactions in MEG/EEG source space: A note of caution on inter-areal coupling measures, *NeuroImage* **173**, 632 (2018).
- [131] T. Donoghue, M. Haller, E. J. Peterson, P. Varma, P. Sebastian, R. Gao, T. Noto, A. H. Lara, J. D. Wallis, R. T. Knight *et al.*, Parameterizing neural power spectra into periodic and aperiodic components, *Nat. Neurosci.* **23**, 1655 (2020).
- [132] J. Samaha and M. X. Cohen, Power spectrum slope confounds estimation of instantaneous oscillatory frequency, *NeuroImage* **250**, 118929 (2022).
- [133] L. E. Wilson, J. da Silva Castanheira, and S. Baillet, Time-resolved parameterization of aperiodic and periodic brain activity, *bioRxiv* (2022), doi: 10.1101/2022.01.21.477243.